Thermochromic undoped and Mg-doped VO_2 thin films and nanoparticles: Optical properties and performance limits for energy efficient windows

Shu-Yi Li,[a] Gunnar A. Niklasson, and Claes G. Granqvist

Department of Engineering Sciences, The Ångström Laboratory, Uppsala University, P.O. Box 534, SE-75121 Uppsala, Sweden

Undoped and Mg-doped thermochromic VO_2 films with atom ratios $z \equiv Mg/(Mg + V)$ of $0 \leq z < 0.21$ were deposited by reactive DC magnetron sputtering onto heated glass and carbon substrates. Elemental compositions were found by Rutherford backscattering spectrometry. Optical constants were determined from transmittance and reflectance measurements and were used for modeling the optical properties of thin films and dilute nanoparticle composite layers below and above the critical temperature for thermochromic switching between a low-temperature infrared transparent state and a high-temperature infrared reflecting or absorbing state. Mg-doped *films* showed superior luminous transmittance T_{lum} and solar transmittance modulation ΔT_{sol} compared to undoped VO_2 films, and both of these parameters could be further enhanced by anti-reflection. VO_2-containing *nanocomposites* had much larger values of T_{lum} and ΔT_{sol} than VO_2-based films. Mg-doping was found to erode the properties of the nanocomposites. Approximate performance limits are given on T_{lum} and ΔT_{sol} for thermochromic VO_2 films, with and without Mg doping and antireflection coating, and also for VO_2-containing dilute nanocomposites.

---

[a] Corresponding author; electronic mail: Shuyi.Li@angstrom.uu.se.

I. INTRODUCTION

Optical constants were determined for sputter-deposited undoped and Mg-doped thermochromic VO_2 films. These data were used in a comprehensive modeling study on luminous transmittance T_{lum} and achievable solar transmittance modulation ΔT_{sol} for different doping levels in films and dilute nanoparticle composites. The overarching goal is to assess VO_2-based materials for energy efficient fenestration, and the present paper is a sequel to earlier ones.[1–10]

Vanadium dioxide is a well known thermochromic material.[11] It undergoes a first-order metal-to-insulator transition, accompanied by a crystal structure transformation from monoclinic (M_1) to tetragonal rutile, at a critical temperature $\tau_c \approx 68$ °C. Below this temperature, at $\tau < \tau_c$, VO_2 is semiconducting and infrared transmitting, whereas it is metallic and infrared reflecting at $\tau > \tau_c$. As τ_c is rather close to room temperature, VO_2-based materials are of interest for applications on energy efficient windows,[12–19] specifically for passively modulating the solar energy throughput depending on temperature. The potential energy saving can be high, especially in warm climates.[20–22] However VO_2 needs a number of modifications in order to be useful in practical windows-related applications: thus τ_c should be lowered to room temperature, and T_{lum} as well as ΔT_{sol} should be enhanced.[7]

Doping is a well-established way to decrease τ_c,[23] with tungsten as the superior dopant capable of reducing τ_c by as much as ~25 °C/at.% W for well-crystallized films, made by a variety of techniques,[7] without severely deteriorating the optical performance.[24] Magnesium doping was found to be able to increase T_{lum} and to simultaneously decrease τ_c by ~3 °C/at.% Mg;[1,25] the boost in optical performance was seen to be connected with band gap widening and concomitant lowering of the spectral absorptance in the luminous wavelength range.[8,10] These features could be reconciled with hybrid functional calculations.[10] Fluorine doping is another way to enhance T_{lum}.[26–29] Furthermore, antireflection (AR) coatings are able to improve T_{lum} and ΔT_{sol}, and especially good properties have been reported for five-layer coatings of alternating TiO_2 and VO_2.[2,3]

Recent modeling studies on "nanothermochromics"[4,5] have shown that VO_2 nanoparticles can offer significantly higher values of T_{lum} and ΔT_{sol} than films, and these new possibilities have led to a burst of research on such nanoparticles.[6,9,19,22,25,30–34] Doped VO_2 nanoparticles are of interest since they may be able to yield reduced values of τ_c, and Mg-doped VO_2

nanoparticles have demonstrated a potential for improving T_{lum} although with some depression of ΔT_{sol}.[25]

This paper is outlined as follows: Section II reports on the samples and treats sputter deposition, compositional and structural data, and optical characterization and properties; this section also contains a discussion of sample quality which—as found in recent work of ours[9]—may be critically dependent on several aspects of the thin film preparation. Section III contains results and discussions for undoped and Mg-doped VO_2 thin films without and with AR coatings as well as for nanoparticle composites containing the same VO_2-based materials. Section IV, finally, summarizes the main findings and presents them in a pictorial way that allows a straight forward comparison of several different types of VO_2-based materials with regard to their potential applicability in energy efficient fenestration.

II. SAMPLE PREPARATION AND CHARACTERIZATION

A. Sputter deposition

Thin films of Mg-doped and pure VO_2 were prepared on glass and carbon substrates by reactive DC magnetron sputtering in a deposition system based on a Balzers UTT 400 unit. The chamber was initially pumped down to 6.3×10^{-7} mbar, and 80 ml/min of argon and 5 ml/min of oxygen (both 99.997%) were then introduced through mass-flow-controlled gas inlets so that the total pressure was maintained at 1.2×10^{-2} mbar during the deposition. Co-sputtering was performed from 5-cm-diameter targets of vanadium (99.5%) at a power of 172 W and Mg (99.9%) at a power of 0 to 57 W onto substrates kept at ~450 °C. Clamps were used to ensure good mechanical contact between substrates and heater. More than forty samples were grown to thicknesses in the range $40 < d < 100$ nm at a rate of ~0.06 nm/s. The value of d was measured with a Bruker DektakXT profilometer and was further confirmed with optical analysis. Some of the as-deposited samples displayed metallic-like properties and were post-annealed at 450 °C in an oxygen atmosphere of 1.3×10^{-2} mbar for 15 to 60 min.

B. Compositional and structural characterization

The elemental compositions of samples deposited on carbon substrates were evaluated using Rutherford backscattering spectrometry (RBS) with 2 MeV ^{4}He ions backscattered at an angle of 170°. Data were then extracted from analyses based on iterative least-square fitting to

experimental spectra by use of the SIMNRA program.[35] Two examples of this evaluation are shown in Fig. 1. The various samples were found to have atom ratios $z \equiv \mathrm{Mg}/(\mathrm{Mg} + \mathrm{V})$ in the interval $0 \leq z < 0.21$. Eight samples contained Si and were excluded from the analysis in the present work but were discussed elsewhere.[8] Film density ρ was evaluated from RBS data and d.

Nanostructural information was obtained by scanning electron microscopy (SEM) using a LEO 1550 FEG Gemini instrument with an acceleration voltage of 5 to 15 kV and using an in-lens detector. Figure 2 shows characteristic data for films with two values of z. A SEM image of an undoped VO_2 film was reported before.[9]

C. Optical characterization techniques and properties

Spectral and temperature-dependent normal transmittance $T(\lambda,\tau)$ and near-normal reflectance from the surface side $R_s(\lambda,\tau)$ and back side $R_b(\lambda,\tau)$ of the samples were measured using a single-beam spectrophotometer devised for absolute measurements[36] and a Perkin–Elmer Lambda 900 double-beam spectrophotometer equipped with a $BaSO_4$-coated integrating sphere. Data were recorded in the wavelength range $300 < \lambda < 2500$ nm, encompassing luminous light at $400 < \lambda < 700$ nm and near-infrared (NIR) radiation at $700 < \lambda < 2500$; measurements were performed at room temperature and ~100 °C. Optical constants n and k were obtained by simulating the complex dielectric functions $\varepsilon = \varepsilon_1 + i\varepsilon_2$ with oscillator models and fitting the experimental data on R_s, R_b and T to calculated spectra using commercial software.[37] A similar approach has been used in earlier work.[8,9,38] Some of the samples had too large surface roughness to give satisfactory fits under the constraints imposed by this analysis and are not considered below. The optical constants for the remaining 22 samples were obtained from

$$n = \left[\frac{1}{2}\left((\varepsilon_1^2 + \varepsilon_2^2)^{1/2} + \varepsilon_1\right)\right]^{1/2}, \tag{1}$$

$$k = \left[\frac{1}{2}\left((\varepsilon_1^2 + \varepsilon_2^2)^{1/2} - \varepsilon_1\right)\right]^{1/2}. \tag{2}$$

Figure 3 shows experimental and fitted spectra for five samples, which are discussed in detail below, whose values of z, d and ρ are given in Table I. The samples exhibit typical behavior of VO_2-based films: the semiconducting state shows high transparency in the NIR, as seen in Fig. 3(c), and the metallic state has a reflectance that rises monotonically for increasing wavelength in the NIR as shown in Figs. 3(d) and (e), except for the sample with z

= 0.088. By comparing the reflectance in the semiconducting state [Figs. 3(a) and (b)] and metallic state [Figs. 3(d) and (e)], one can notice that the reflectance modulation in the NIR is smaller for Mg-doped VO_2 films than for undoped VO_2 films. It is also apparent that the onsets of transmittance shift towards shorter wavelengths when the Mg doping is large.

Data of the kind reported in Fig. 3 were used to extract optical constants for undoped and Mg-doped VO_2 films at $\tau < \tau_c$ and $\tau > \tau_c$, as reported in Fig. 4. For the semiconducting state (Fig. 4a), n and k curves show similar trends for all Mg contents. The data are rather wavelength-independent in the NIR, except for the very broad maximum around ~1000 nm in the case of k. The peak in k at the shortest wavelengths signifies the strong optical absorption due to inter-band transitions at the band gap energy E_g, where $1.6 < E_g < 2.6$ eV.[8,10] The value of k for luminous light, as well as the level of the plateau in the NIR data for n, shows a tendency to decrease for Mg-doped VO_2 films, but it is difficult to ascertain a systematic relationship. For the metallic state (Fig. 4b), it can be seen that k increases with increasing wavelength in the NIR, and the same is true for n at $\lambda > 1000$ nm. In the case of undoped VO_2, k exhibits a marked metallic behavior and surpasses the value of n for $\lambda > 1100$ nm. The metallic feature is weaker in Mg-doped VO_2, which can be reconciled with the reflectance data in the metallic state shown in Figs. 3(d) and (e). Our results for undoped VO_2 films are consistent with literature data,[3,24,39–41] as shown in detail elsewhere.[9]

It can be inferred from Fig. 3 and Table I that n and ρ are correlated. Evaluations performed for λ being 550, 1000 and 2500 nm showed an approximate linear relationship according to

$$n = \kappa + \zeta\rho, \tag{3}$$

with $\kappa = 1.2 \pm 0.1$ and $\zeta \sim 0.32$ m^3/kg.

D. On sample quality and reproducibility

It is evident from the optical data in Figs. 3 and 4 that substantial scattering exists for VO_2-based thin films with nominally the same composition and deposited with similar parameters. This observation leads to considerations of sample quality and reproducibility, which clearly are of great importance and—in our opinion—have not received sufficient attention in most prior work. These issues were addressed, however, in a recent study of ours whose main goal was to elucidate the growth conditions for sputter deposited VO_2 films and nanorods.[9] Five different deposition parameters were identified and found to be crucial:

(*i*) The geometry for inlet of the reactive gas during sputter deposition affected the roughness and grain structure of the films. In the present work we used conditions denoted (a) in our earlier study,[9] which were then found to lead to compact films with a density that was about 11% lower than the bulk value for VO_2. The critical importance of the oxygen partial pressure and flow rate has been demonstrated repeatedly in earlier work.[42–46]

(*ii*) The film thickness was important, and a large value of *d* promoted the formation of surface nanostructures, as also seen elsewhere.[47,48] More generally, the surface of a VO_2 film may be different from its main part[49] and the same may be true for the substrate/film interface.[50]

(*iii*) The substrate temperature during deposition played a role, as found also by others,[51–53] and a high value could lead to surface nanofeatures.

(*iv*) Substrate roughness promoted the development of film roughness.

(*v*) Seed layers could yield pronounced nanostructures, as investigated in detail for the case of gold seeds in the earlier investigation[9] where they were found to lead to nanorod formation.

For the present work, one should also consider the role of Mg doping as a potential source for influencing the growth of VO_2-based films. Another factor affecting the reproducibility may be thermal stress induced in the film during deposition and subsequent cooling.[54, 55]

Considering these uncertainties, it may not be surprising that our samples show significant scattering in their optical properties, despite our sustained efforts to prepare the films under as stringent process control as possible. The data encapsulated in Eq. (3) are interesting in this context and point at the significance of porosity across the entire VO_2-based films rather than a dominating influence of surface roughness. In order to compensate for the limited sample reproducibility, we investigated a sufficiently large number of samples in order to reach trustworthy results and conclusions.

III. OPTICAL MODELING: RESULTS AND DISCUSSION

Thin films and nanoparticle composite layers were characterized in terms of their wavelength-integrated luminous and solar transmittance. These properties were obtained from

$$T_{\mathrm{lum,sol}}(\tau) = \int d\lambda\ \varphi_{\mathrm{lum,sol}}(\lambda)\ T(\lambda,\tau) \,/\, \int d\lambda\ \varphi_{\mathrm{lum,sol}}(\lambda)\ , \qquad (4)$$

where φ_{lum} is the spectral sensitivity of the light-adapted human eye[56] and φ_{sol} is the solar irradiance spectrum for air mass 1.5 (the sun at 37° above the horizon).[57] The thermochomic performance, and its relevance for energy efficient fenestration, was specified by T_{lum} for $\tau < \tau_c$ and $\tau > \tau_c$, T_{sol} for $\tau < \tau_c$ and $\tau > \tau_c$, and ΔT_{sol} defined by

$$\Delta T_{sol} \equiv T_{sol}(\tau < \tau_c) - T_{sol}(\tau > \tau_c) \quad . \tag{5}$$

A. Thin films

Calculations based on Fresnel's equations[58] were used to derive $T(\lambda,\tau)$ for VO_2-based thin films with $0 < d < 200$ nm and backed by glass plates characterized by a refractive index 1.5. The input data were our optical constants for all 22 samples, some of which were shown in Fig. 4.

Figure 5 shows data for a fixed film thickness of 50 nm. The influence of Mg-doping is illustrated for $T_{lum}(\tau < \tau_c)$, $T_{lum}(\tau > \tau_c)$ and ΔT_{sol} in panels (a), (b) and (c), respectively. The values of T_{lum}, reported in panels (a) and (b), show a general tendency to increase for increasing amount of Mg, although there is significant scattering among the data points especially for small doping levels. Concerning ΔT_{sol}, Fig. 5(c) indicates a decreasing trend as z is increased. These findings are in good agreements with literature data[1,25] showing that T_{lum} and ΔT_{sol} display opposite trends with regard to Mg-doping. In particular, the band gap widening that occurs gradually for increasing z leads to a boost in T_{lum}.

The lowering of the luminous absorption in Mg-doped VO_2 films indicates that they may outperform undoped VO_2 films for both T_{lum} and ΔT_{sol} if given a judicious choice of thickness. The effect of film thickness in the $0 < d < 200$ nm interval is elucidated in Fig. 6, where panels (a) and (b) refer to $T_{lum}(\tau < \tau_c)$ *vs* ΔT_{sol} and $T_{lum}(\tau > \tau_c)$ *vs* ΔT_{sol}, respectively. All curves start at the top left of the figure with $d = 0$, $\Delta T_{sol} = 0$ and $T_{lum} \approx 92\%$ and proceed to the bottom right with $d = 200$ nm. For clarity, the data are categorized in four groups according to Mg content: $z = 0$, $0 < z < 0.06$, $0.06 < z < 0.11$, and $0.11 < z < 0.21$.

We first consider data for undoped VO_2. Requiring $\Delta T_{sol} > 5\%$ leads to T_{lum} around 40% or less, and demanding $\Delta T_{sol} > 10\%$ forces T_{lum} to be smaller than ~30%. Such a moderate thermochromic performance is typically expected with undoped VO_2 films, although the detailed numbers can vary somewhat depending on the individual set of n and k chosen for analysis. It is hence clear that it is desirable to seek means to improve VO_2 films.

Among the data for Mg-doped VO_2 films, those for $0.11 < z < 0.21$ show poor performance, and these "overdoped" samples are not considered further. The remaining samples follow the same trend irrespectively of being semiconducting or metallic: there is an initial rapid drop of T_{lum}, which is particularly abrupt for ΔT_{sol} being 2 to 4%, followed by another less pronounced drop of T_{lum} when ΔT_{sol} is around 8 to 10%. For solar modulations between these two intervals, it is seen that T_{lum} remains rather unchanged. The reason for this constancy is to be found in optical interference, and it appears that destructive interference lowers the reflectance to more or less balance out the increased optical absorption associated with the larger film thickness. Another important observation from Fig. 6 is that the data for the great majority of the Mg-doped VO_2 films lie to the upper right of the data for pure VO_2, implying that Mg doping leads to a significant enhancement of T_{lum} and ΔT_{sol}. One can also draw the provisional conclusion that the best samples have $z < 0.06$. Specifically requiring $\Delta T_{sol} = 10\%$, which may be a performance limit for practically useful thermochromic fenestration, one can achieve $T_{lum}(\tau < \tau_c) \approx 45\%$ and a slightly lower value at $\tau > \tau_c$, whereas an undoped VO_2 film only yields $T_{lum} \sim 30\%$ at best.

B. Thin films with antireflection coatings

AR coatings can improve T_{lum} and ΔT_{sol}, as is well known, and studies have been reported for SiO_2/VO_2,[59–62] TiO_2/VO_2,[18,61,63] ZrO_2/VO_2,[64] $SiO_x/VO_2/SiO_x$,[40] $TiO_2/VO_2/TiO_2$,[2,3,65] and $TiO_2/VO_2/TiO_2/VO_2/TiO_2$.[2,3] Infrared-optical properties have been optimized in films of ITO/VO_2 and ITO/VO_2/ITO.[66] An AR coating can serve also to prevent the oxidation of VO_2, as shown for base layers of TiO_2 (Ref. 67) and top layers of CeO_2 (Ref. 68) and Al_2O_3,[69] and also to lower the thermal emittance as found for ZnO:Al/VO_2.[70] A survey of earlier work has been given in the literature.[19] We investigated the effect of AR coatings with thicknesses in the range $0 < d_{AR} < 300$ nm, characterized by a refractive index $n_{AR} = 1.5$ (typical for SiO_2 and many polymers), positioned on top of VO_2-based films with different values of z and d as specified in the first two columns in Table II. The outcomes of the calculations were visualized as trajectories in plots of $T_{lum}(\tau < \tau_c)$ *vs* ΔT_{sol} and $T_{lum}(\tau > \tau_c)$ *vs* ΔT_{sol}, as shown in Fig. 7. It is apparent that T_{lum} and T_{sol} vary significantly when d_{AR} is changed, and that there are particular magnitudes of d_{AR} that yield favorable combinations of these parameters. We selected the points indicated by circles in Fig. 7, which correspond to the values of d_{AR} in the third column in Table II. Clearly this technique involves some degree of subjectivity but was deemed appropriate for giving a good overall picture of the improvements of the optical properties that are feasible with AR coatings. Calculations were also done for $n_{AR} = 2.1$,

which is typical for sputter-deposited TiO_2 films.[71] However, the results were not significantly better than those for n_{AR} = 1.5 and are not further discussed here.

Table II shows data from the computations. It is evident that AR treatments can significantly improve T_{lum} by up to ~8% in absolute value, while adding 2 to 3% to ΔT_{sol}. A well-chosen set of parameters can offer ΔT_{sol} = 9.2%, with $T_{lum}(\tau < \tau_c)$ and $T_{lum}(\tau > \tau_c)$ reaching 59.3% and 57%, respectively. Alternatively, one can push ΔT_{sol} to 12.8% and maintain $T_{lum}(\tau < \tau_c)$ and $T_{lum}(\tau > \tau_c)$ at 47.5% and 44%, respectively. Even higher solar modulation, with ΔT_{sol} = 15.4%, is achievable but at the expense of having T_{lum} ~ 30%.

The results in Table II are consistent with the best data for TiO_2/VO_2 films in the literature, reported recently by Chen *et al.*[61] who found $\Delta T_{sol} \approx 15\%$ together with $T_{lum}(\tau < \tau_c)$ and $T_{lum}(\tau > \tau_c)$ being 49.5% and 45%, respectively.

C. Nanothermochromics: VO_2 nanospheres embedded in a dielectric medium

The modeling considers VO_2 nanoparticles embedded in a glass or polymer-like dielectric medium characterized by the dielectric constant ε_m = 2.25 (refractive index 1.5). The optical properties of such a composite layer can be described with effective medium theory, assuming nanoparticle sizes that are much smaller than the wavelength. In the same manner as in earlier work,[4,72,73] we derive an effective dielectric function ε^{MG} from Maxwell–Garnett theory[74] according to

$$\varepsilon^{MG} = \varepsilon_m \frac{1+\frac{2}{3} f\alpha}{1-\frac{1}{3} f\alpha} \quad , \tag{5}$$

where f represents the filling factor (*i.e.*, volume fraction) of VO_2 particles and is taken to be 0.01 for the dilute material of present interest. The parameter α is given for spherical particles by

$$\alpha = \frac{\varepsilon_p - \varepsilon_m}{\varepsilon_m + \frac{1}{3}(\varepsilon_p - \varepsilon_m)} \quad , \tag{6}$$

where ε_p is the dielectric function of the VO_2 particles. VO_2 has an exceptionally small mean free path,[75–78] which is not large enough to impart any particle size dependence, and hence it is appropriate to use the dielectric functions obtained from films as input data for ε_p. Finally

ε^{MG} for VO_2-based films with different Mg contents was used as an input for computations of $T(\lambda,\tau)$ and $R(\lambda,\tau)$ for layers comprising nanoparticle composites. These calculations used Fresnel's equations in the same way as for films. The layer thickness for the nanocomposites was varied in the $0 < d_{nc} < 20$ μm range to enable comparison with data for films containing the same amount of VO_2-based material and shown above.

Figure 8 reports data for a fixed layer thickness of 5 μm in the same way as for the 50-nm-thick films in Fig. 5. It is evident from panels (a) and (b) that $T_{lum}(\tau < \tau_c)$ and $T_{lum}(\tau > \tau_c)$ both rise for increasing values of z although there is a significant amount of scattering of data for nanocomposites containing metallic VO_2-based particles. It is noteworthy that all of the transmittance values exceed 55%, *i.e.*, they are much larger than the corresponding values shown in Fig. 5. Data on ΔT_{sol}, reported in Fig. 8(c), show that this parameter is two to three times larger than in films, and it is also apparent that ΔT_{sol} drops for increasing Mg contents. The results in Fig. 8 are in line with earlier findings[4] that the values of T_{lum} and ΔT_{sol} are much higher for nanoparticle composites than for thin films. It is apparent that T_{lum} and ΔT_{sol} exhibit opposite trends for increasing Mg contents.

Figure 9 shows the effect of layer thicknesses in the $0 < d_{nc} < 20$ μm range for $T_{lum}(\tau < \tau_c)$ *vs* ΔT_{sol} and $T_{lum}(\tau < \tau_c)$ *vs* ΔT_{sol} in panels (a) and (b), respectively. This figure allows a direct comparison with data for thin films in Fig. 6. It is evident that the general picture regarding nanoparticle-containing layers is very different from the one for thin films, and the layers with nanoparticles of undoped VO_2 in general outperform the layers with Mg-doped VO_2. Specific data for two different layers are given in Table III in order to allow comparisons with results for AR-coated VO_2-based films in Table II.

The superior performance of the nanocomposite layers should be underscored and, for example, Fig. 9 shows that $T_{sol} = 10\%$ can be obtained with $T_{lum}(\tau < \tau_c) \sim 82\%$ and $T_{lum}(\tau > \tau_c) \sim 77.5\%$, whereas films then have $T_{lum} < 35\%$, and that a value of T_{sol} as large as 20%—which is unattainable for films—can be reached with $T_{lum}(\tau < \tau_c) \sim 66\%$ and $T_{lum}(\tau > \tau_c) \sim 57\%$.

The reason for the qualitative difference between nanoparticle composite layers and thin films can be unraveled from calculations of $T(\lambda,\tau)$ and $R(\lambda,\tau)$, as reported in Fig. 10 for layers incorporating nanoparticles of undoped and Mg-doped VO_2 with $z = 0.055$ and having the thicknesses 1, 3, and 10 μm. Three things deserve attention and explain the superior performance of the undoped VO_2 nanoparticles: (*i*) the optical properties for luminous light are similar for the two types of materials, and Mg doping does not seem to offer any significant advantage, (*ii*) the positive influence of optical interference manifested in the films

is absent in the nanoparticle composite layers, and (*iii*) the plasmon resonance in the NIR is largest in pure VO_2, which follows from its stronger metallic behavior, so that the modulation of the absorption is then strongest at τ_c. The net effect is that the larger value of ΔT_{sol} for undoped VO_2 outweighs the increase of T_{lum} by Mg-doping in the case of dilute nanoparticle composites.

IV. SUMMARY AND CONCLUSION

This study has offered a comprehensive view on thermochromc VO_2-based materials with regard to applications in energy efficient windows. We sputter deposited undoped and Mg-doped VO_2 films and determined their optical constants, which were subsequently used in model computations for optical properties of undoped and Mg-doped VO_2 films and dilute nanoparticle composite layers with different thicknesses. It was found from computational results that Mg-doped VO_2 films with Mg/(Mg + V) < 0.06 and judiciously chosen thicknesses can have much improved luminous transmittance and solar energy modulation than pure VO_2 films. The addition of single-layer anti-reflection coatings on the top of the VO_2-based films was shown to further enhance the performance of Mg-doped films. Modeling of nanoparticle composites suggested that undoped VO_2 nanoparticles are more favorable than Mg-doped ones.

Figure 11 gives a pictorial description of the results of our investigation and delineates values of $T_{lum}(\tau < \tau_c)$ and ΔT_{sol} that are achievable with different VO_2-based materials. Various ranges—whose boundaries should not be understood as written in stone—are given for films of undoped and Mg-doped VO_2 without and with a single antireflection coating, and also for nanoparticle composites containing undoped and Mg-doped nanospheres. Non-spherical nanoparticle shapes as well as core-shell structures may improve the performance marginally[4,5] but will not lead to any significant change of Fig. 11. Multilayer structures incorporating more than one VO_2-layer are not encompassed by Fig. 11 and, as shown for $TiO_2/VO_2/TiO_2/VO_2/TiO_2$ films with optimized thicknesses,[2,3] can show a performance that is better than for a single undoped and antireflected VO_2 film, and still better data may be expected for structures containing more than one doped VO_2 film. However, these possible refinements will not alter the overriding result for VO_2-based materials, namely that nanoparticle composites are superior to films.

ACKNOWLEDGEMENTS

Financial support was received from the Swedish Research Council and from the European Research Council under the European Community's Seventh Framework Program (FP7/2007–2013)/ERC Grant Agreement No. 267234 (GRINDOOR). We acknowledge assistance with RBS measurements from Daniel Primetzhofer, Pia C. Lansåker, Anders Hallén, Göran Possnert, Per Pettersson, and the staff of the Tandem Accelerator Laboratory at Uppsala University.

REFERENCES

[1]N. R. Mlyuka, G. A. Niklasson, and C. G. Granqvist, Appl. Phys. Lett. **95**, 171909 (2009).

[2]N. R. Mlyuka, G. A. Niklasson, and C. G. Granqvist, Sol. Energy Mater. Sol. Cells **93**, 1685 (2009).

[3]N. R. Mlyuka, G. A. Niklasson and C. G. Granqvist, Phys. Status Solidi A **206**, 2155 (2009).

[4]S.-Y. Li, G. A. Niklasson, and C. G. Granqvist, J. Appl. Phys. **108**, 063525 (2010).

[5]S.-Y. Li, G. A. Niklasson, and C. G. Granqvist, J. Appl. Phys. **109**, 113515 (2011).

[6]S.-Y. Li, G. A. Niklasson, and C. G. Granqvist, Appl. Phys. Lett. **99**, 131907 (2011).

[7]S.-Y. Li, G. A. Niklasson, and C. G. Granqvist, Thin Solid Films **520**, 3823 (2012).

[8]S.-Y. Li, N. R. Mlyuka, D. Primetzhofer, A. Hallén, G. Possnert, G. A. Niklasson, and C. G. Granqvist, *Band Gap Widening in Thermochromic Mg-doped VO_2 Thin Films: Quantitative data Based on Optical Absorption*, submitted to Appl. Phys. Lett. (2013).

[9]S.-Y. Li, K. Namura, M. Suzuki, G. A. Niklasson, and C. G. Granqvist, J. Appl. Phys. **114**, 033516 (2013).

[10]S. Hu, S.-Y. Li, R. Ahuja, C. G. Granqvist, K. Hermansson, G. A. Niklasson, and R. H. Scheicher, Appl. Phys. Lett. **101**, 201902 (2012).

[11]F. J. Morin, Phys. Rev. Lett. **3**, 34 (1959).

[12]C.B. Greenberg, Thin Solid Films **110**, 73 (1983).

[13]G. V. Jorgenson and J. C. Lee, Sol. Energy Mater. **14**, 205 (1986); in *Large-Area Chromogenics: Materials and Devices for Transmittance Control,* edited by C. M. Lampert and C. G. Granqvist (SPIE Optical Engineering Press, Bellingham, WA, 1990), SPIE Institutes for Advanced Optical Technologies, Vol. IS 4, pp. 142–159.

[14]S. M. Babulanam, T. S. Eriksson, G. A. Niklasson, and C. G. Granqvist, Sol. Energy Mater. **16**, 347 (1987).

[15]I. P. Parkin and T. D. Manning, J. Chem. Edu. **83**, 393 (2006).

[16]I. P. Parkin, R. Binions, C. Piccirillo, C. S. Blackman, and T. D. Manning, J. Nano. Res. **2**, 1 (2008).

[17]G. B. Smith and C. G. Granqvist, *Green Nanotechnology: Solutions for Sustainability and Energy in the Built Environment* (CRC Press, Boca Raton, FL, 2010).

[18]Z. Zhang, Y. Gao, H. Luo, L. Kang, Z. Chen, J. Du, M. Kanehira, Y. Zhang, and Z. L. Wang, Energy Environ.Sci. **4**, 4290 (2011).

[19]A. Taylor, I. Parkin, N. Noor, C. Tummeltshammer, M. S. Brown, and I. Papakonstantinou, Opt. Expr. **21**, A750 (2013).

[20]M. Saeli, C. Piccirillo, I. P. Parkin, R. Binions, and I. Ridley, Energy Buildings **42**, 1666 (2010).

[21]M. Saeli, C. Piccirillo, I. P. Parkin, I. Ridley, and R. Binions, Sol. Energy. Mater. Sol. Cells **94**, 141 (2010).

[22]Y. Gao, H. Luo, Z. Zhang, L. Kang, Z. Chen, J. Du, M. Kanehira, and C. Cao, Nano Energy **1**, 221 (2012).

[23]J. B. Goodenough, J. Solid State Chem. **3**, 490 (1971).

[24]M. Tazawa, P. Jin, and S. Tanemura, Applied Optics **37**, 1858 (1998).

[25]J. Zhou, Y. Gao, X. Liu, Z. Chen, L. Dai, C. Cao, H. Luo, M. Kanahira, C. Sun, and L. Yan, Phys. Chem. Chem. Phys. **15**, 7505 (2013).

[26]K. A. Khan and C. G. Granqvist, Appl. Phys. Lett. **55**, 4 (1989).

[27]W. Burkhardt, T. Christmann, B. K. Meyer, W. Niessner, D. Schalch, and A. Scharmann, Thin Solid Films **345**, 229 (1999).

[28]W. Burkhardt, T. Christmann, S. Franke, W. Kriegseis, D. Meister, B. K. Meyer, W. Niessner, D. Schalch, and A. Scharmann, Thin Solid Films **402**, 226 (2002).

[29]P. Kiri, M. E. A. Warwick, I. Ridley, and R. Binions, Thin Solid Films **520**, 1363 (2011).

[30]S. Ji, F. Zhang, and P. Jin, Sol. Energy Mater. Sol. Cells **95**, 3520 (2011).

[31]Y. Li, S. Ji, Y. Gao, H. Luo, and M. Kanehira, Sci. Rep. **3:** 1370 (2013c); doi:10.1038/srep01370 (13 pages).

[32]Y. Gao, S. Wang, H. Luo, L. Dai, C. Cao, Y. Liu, Z. Chen, and M. Kanehira, Energy Environ. Sci. **5**, 6104 (2012).

[33]Y. Gao, S. Wang, L. Kang, Z. Chen, J. Du, X. Liu, H. Luo, and M. Kanehira, Energy Environ. Sci. **5**, 8234 (2012).

[34]J. Zimmer, A. Wixforth, H. Karl, and H. J. Krenner, Appl. Phys. Lett. **100**, 231911 (2012).

[35]M. Mayer, AIP Conf. Proc. **475**, 541 (1999).

[36]P. Nostell, A. Roos, and D. Ronnow, Rev. Sci. Instrum. **70**, 2481 (1999).

[37]M. Theiss, *Hard and Software for Optical Spectroscopy*, Dr.-Bernhard-Klein-Str. 110, D-52078 Aachen, Germany, 2002; http://www.mtheiss.com.

[38]V. Panayotov and I. Konstantinov, Appl. Opt. **30**, 2795 (1991).

[39]H. W. Verleur, A. S. Barker, and C. N. Berglund, Phys. Rev. **172**, 788 (1968).

[40]H. Kakiuchida, P. Jin, and M. Tazawa, Sol. Energy Mater. Sol. Cells **92**, 1279 (2008).

[41]J. B. Kana Kana, J. M. Ndjaka, G. Vignaud, A. Gibaud, and M. Maaza, Opt. Commun. **284**, 807 (2011).

[42]B. D. Gauntt, E. C. Dickey, and M. W. Horn, J. Mater. Res. **24**, 1590 (2009).

[43]T.-W. Chiu, K. Tonooka, and N. Kikuchi, Thin Solid Films **518**, 7441 (2010).

[44]C. Venkatasubramanian, O. M. Cabarcos, W. R. Drawl, D. L. Allara, S. Ashok, M. W. Horn, and S. S. N. Bharadwaja, J. Vac. Sci. Technol. A **29**, 061504 (2011).

[45]L. L. Fan, Y. F. Wu, C. Si, C. W. Zou, Z. M. Qi, L. B. Li, G. Q. Pan, and Z. Y. Wu, Thin Solid Films **520**, 6124 (2012).

[46]Y. H. Tian, S. S. Pan, Y. Y. Luo, and G. H. Li, Sci. Adv. Mater. **4**, 351 (2012).

[47]G. Xu, P. Jin, M. Tazawa, and K, Yoshimura, Appl. Surf. Sci. **244**, 449 (2005).

[48]X.-B. Wei, Z.-M. Wu, X.-D. Xu, T. Wang, J.-J. Tang, W.-Z. Li, Y.-D. Jiang, J. Phys. D: Appl. Phys. **41**, 055303 (2008).

[49]W. Yin, K. G. West, J. W. Lu, Y. Pei, S. A. Wolf, P. Reinke, and Y. Sun, J. Appl. Phys. **105**, 114322 (2009).

[50]J. Ma, G. Xu, L. Miao, M. Tazawa, and S. Tanemura, Jpn. J. Appl. Phys. **50**, 020215 (2011).

[51]E. E. Chain, J. Vac, Sci. Technol. A **4**, 432 (1986).

[52]P. Jin, K. Yoshimura, and S. Tanemura, J. Vac. Sci. Technol. A **15**, 1113 (1997).

[53]D.-H. Youn, J.-W. Lee, B.-G. Chae, H.-T. Kim, S.-L. Maeng, J. Appl. Phys. **95**, 1407 (2004).

[54]Y. NingYi, L. Jinhua, H.L.W. Chan, L. Chenglu, Appl. Phys. A **78**, 777 (2004).

[55]F. Beteille, L. Mazerolles, J. Livage, Mater. Res. Bull. **34**, 2177 (1999).

[56]G. Wyszecki and W. S. Stiles, *Color Science: Concepts and Methods, Quantitative Data and Formulae,* 2nd ed. (Wiley, New York, 2000).

[57]ASTM G173-03 Standard Tables of Reference Solar Spectral Irradiances: Direct Normal and Hemispherical on a 37° Tilted Surface, *Annual Book of ASTM Standards* (American Society for Testing and Materials, Philadelphia, PA, USA, 2008), Vol. 14.04; http://rredc.nrel.gov/solar/spectra/am1.5.

[58]M. Born and E. Wolf, *Principles of Optics*, 7th ed. (Cambridge University Press, Cambridge, UK, 1999).

[59]M.-H. Lee and J.-S. Cho, Thin Solid Films **365**, 5 (2000).

[60]M.-H. Lee, Sol. Energy Mater. Sol. Cells **71**, 537 (2002).

[61]Z. Chen, Y. Gao, L. Kang, J. Du, Z. Zhang, H. Luo, H. Miao, and G. Tan, Sol. Energy Mater. Sol. Cells 95, 2677 (2011).

[62]X. Chen, Q. Lv, and X. Yi, Optik **123**, 1187 (2012).

[63]P. Jin, G. Xu, M. Tazawa, and K. Yoshimura, Jpn. J. Appl. Phys. **41**, L278 (2002).

[64]G. Xu, P. Jin, M. Tazawa, and K. Yoshimura, Sol. Energy Mater. Sol. Cells **83**, 29 (2004).

[65]P. Jin, G. Xu, M. Tazawa, and K. Yoshimura, Appl. Phys. A **77**, 455 (2003).

[66]S. T. Heinilehto, J. H. Lappalainen, H. M. Jantunen, and V. Lantto, J. Electroceram. **27**, 7 (2011).

[67]Z. Zhang, Y. Gao, L. Kang, J. Du, H. Luo, J. Phys. Chem. C **114**, 22214 (2010).

[68]S. Saitzek, F. Guinneton, L. Sauques, K. Aguir, and J. R. Gavarri, Opt. Mater. **30**, 407 (2007).

[69]C.G. Granqvist, İ. Bayrak Pehlivan, Y.-X. Ji, S.-Y. Li and G.A. Niklasson, Thin Solid Films, to be published (2014).

[70]L. Kang, Y. Gao, H. Luo, J. Wang, B. Zhu, Z. Zhang, J. Du, M. Kanehira, and Y. Zhang, Sol. Energy Mater. Sol. Cells **95**, 3189 (2011).

[71]J. Rodríguez, M. Gómez, J. Ederth, G. A. Niklasson, and C. G. Granqvist, Thin Solid Films **365**, 119 (2000).

[72]C. G. Granqvist and O. Hunderi, Phys. Rev. B **16**, 3513 (1977).

[73]C. G. Granqvist and O. Hunderi, Phys. Rev. B **18**, 2897 (1978).

[74]J. C. Maxwell–Garnett, Philos. Trans. R. Soc. London, Ser. A **203**, 385 (1904); **205**, 237 (1906).

[75]P. B. Allen, R. M. Wentzcovitch, W. W. Schulz, and P. C. Canfield, Phys. Rev. B **48**, 4359 (1993).

[76]H. S. Choi, J. S. Ahn, J. H. Jung, T. W. Noh, and D. H. Kim, Phys. Rev. B **54**, 4621 (1996).

[77]K. Okazaki, S. Sugai, Y. Muraoka, and Z. Hiroi, Phys. Rev. B **73**, 165116 (2006).

[78]A. Gentle, A. I. Maaroof, and G. B. Smith, Nanotechnology **18**, 025202 (2007).

TABLE I. Data on Mg/(Mg + V) atom ratio, film thickness and film density for samples reported on in Figs. 3 and 4.

Mg/(Mg + V)	Film thickness (nm)	Film density (10^3 kg/m^3)
0	64.5	4.5
0.006	61	2.9
0.024	40	4.9
0.055	49.5	2.9
0.088	79.3	3.6

TABLE II. Luminous transmittance T_{lum}, for temperatures below and above the critical temperature τ_c, and solar energy transmittance modulation ΔT_{sol} for thermochromic Mg-doped VO_2 films with the shown Mg content and thickness d. Data are reported after application of an antireflection coating with the thickness d_{AR} as well as in the absence of antireflection (numbers in parenthesis). Highlighted parameter values are discussed in the main text.

Mg/(Mg + V)	d (nm)	d_{AR} (nm)	ΔT_{sol} (%)	$T_{lum}(\tau < \tau_c)$ (%)	$T_{lum}(\tau > \tau_c)$ (%)
0	70	265	11.6 (8.4)	45.3 (35.1)	41.5 (32.8)
0.006	90	260	**9.2** (7.3)	**59.3** (50.7)	**57** (49.7)
0.024	80	265	12.4 (9.3)	44.6 (36.6)	39 (31.6)
0.055	110	265	**12.8** (10.4)	**47.5** (42.5)	**44** (39.4)
0.055	147.5	95	14.4 (12.3)	37 (30.2)	33.2 (29.7)
0.055	147.5	155	15.4 (12.3)	32.1 (30.2)	29.8 (29.7)

TABLE III. Luminous transmittance T_{lum}, for temperatures below and above the critical temperature τ_c, and solar energy transmittance modulation ΔT_{sol} for nanoparticle composite layers with the thickness d_{nc} and containing 1 vol.% of thermochromic Mg-doped VO_2 nanoparticles having the shown Mg content. Results for undoped VO_2 represent averages of the data for two samples.

Mg/(Mg + V)	d_{nc} (μm)	ΔT_{sol} (%)	$T_{lum}(\tau < \tau_c)$ (%)	$T_{lum}(\tau > \tau_c)$ (%)
0	1	4.6	87.8	86
0	5	16.8	72.4	65.2
0	10	23.7	57	46.5
0.055	1	3.0	88.5	87.4
0.055	5	11.9	75	70.4
0.055	10	18.4	61.2	54

Figure Captions

FIG. 1. Experimental and simulated RBS spectra for VO_2-based films with the shown Mg/(Mg + V) atom ratios. Insets show magnified data due to Mg. Evidence was found for MgO layers on top of the VO_2-based films and/or in between these films and their substrates; these layers in general had a combined thickness that was less than 2% of the total film thickness and are considered insignificant for the compositional analysis.

FIG. 2. SEM images of VO_2-based films with the shown Mg/(Mg + V) atom ratios. Panels (a) and (c) are top views and panels (b) and (d) were imaged at 70° between electron beam and surface normal.

FIG. 3. Experimental and calculated spectral optical data for undoped and Mg-doped thermochromicVO_2 films with the shown Mg/(Mg + V) atom ratios. Reflectance from the surface-coated side and the back side, as well as transmittance, are reported as indicated in the various panels. Upper and lower panels refer to films in semiconducting ($\tau < \tau_c$) and metallic ($\tau > \tau_c$) states, respectively.

FIG. 4. Optical constants, n and k, of undoped and Mg-doped thermochromic VO_2 films with the shown Mg/(Mg+V) atom ratios. Panels (a) and (b) show data for semiconducting ($\tau < \tau_c$) and metallic ($\tau > \tau_c$) states, respectively.

FIG. 5. Luminous transmittance T_{lum} (panels a and b) and solar energy transmittance modulation ΔT_{sol} (panel c) for 50-nm-thick films of undoped and Mg-doped thermochromic VO_2 with the shown Mg/(Mg+V) atom ratios. Panels (a) and (b) show results for semiconducting ($\tau < \tau_c$) and metallic ($\tau > \tau_c$) states, respectively.

FIG. 6. Luminous transmittance T_{lum} *vs* solar energy transmittance modulation ΔT_{sol} for films of undoped and Mg-doped thermochromic VO_2 films with the shown Mg/(Mg+V) $\equiv z$ atom ratios and having film thicknesses from zero to 200 nm. Panels (a) and (b) show results for semiconducting ($\tau < \tau_c$) and metallic ($\tau > \tau_c$) states, respectively.

FIG. 7. Luminous transmittance T_{lum} *vs* solar energy transmittance modulation ΔT_{sol} for films of undoped and Mg-doped thermochromic VO_2 films with Mg/(Mg+V) atom ratios and film thicknesses d given in Table II. The curves evolved from the point marked with an triangle as the thickness d_{AR} of an antireflection layer went from zero to 300 nm. Data are shown for semiconducting ($\tau < \tau_c$) and metallic ($\tau > \tau_c$) states, respectively. Circles indicate data points corresponding to values of d_{AR}, T_{lum} and ΔT_{sol} given in Table II.

FIG. 8. Luminous transmittance T_{lum} (panels a and b) and solar energy transmittance modulation ΔT_{sol} (panel c) for 5-μm-thick nanocomposite layers containing 1 vol.% of undoped and Mg-doped thermochromic VO_2 with the shown Mg/(Mg+V) atom ratios. Panels (a) and (b) show results for semiconducting ($\tau < \tau_c$) and metallic ($\tau > \tau_c$) states, respectively.

FIG. 9. Luminous transmittance T_{lum} *vs* solar energy transmittance modulation ΔT_{sol} for nanocomposite layers containing 1 vol.% of undoped and Mg-doped thermochromic VO_2 with the shown Mg/(Mg+V) atom ratios and having nanoparticle composite thicknesses from zero to 20 μm. Panels (a) and (b) show results for semiconducting ($\tau < \tau_c$) and metallic ($\tau > \tau_c$) states, respectively.

FIG 10. Spectral transmittance T and reflectance R for nanocomposite layers containing 1 vol.% of undoped and Mg-doped thermochromic VO_2 with the shown Mg/(Mg+V) atom ratio and having the stated thicknesses. Panels (a) and (b) show results for semiconducting ($\tau < \tau_c$) and metallic ($\tau > \tau_c$) states, respectively.

FIG. 11. Schematic illustration of achievable performance limits of the shown VO_2-based materials with regard to thermochromic fenestration for energy efficient buildings. Specifically shown are luminous transmittance T_{lum} at low temperature and solar energy transmittance modulation ΔT_{sol} for thin films—including antireflection (AR) coated ones—and dilute nanoparticle composites.

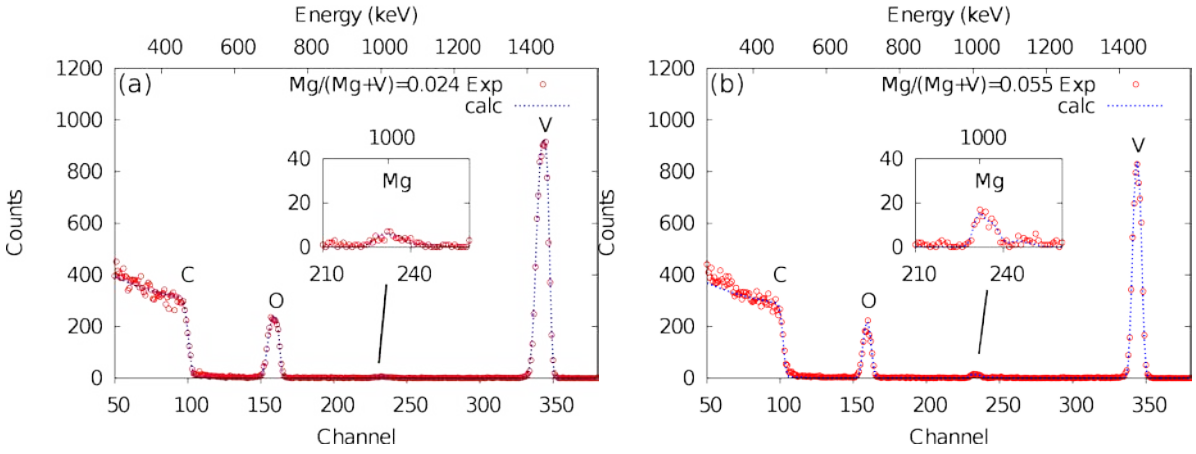

FIG. 1.

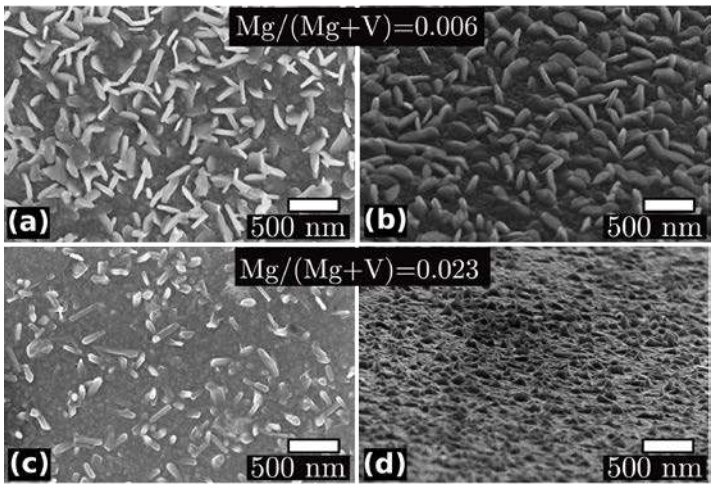
Mg/(Mg+V)=0.006
(a)
500 nm
(b)
500 nm
Mg/(Mg+V)=0.023
(c)
500 nm
(d)
500 nm

FIG. 2.

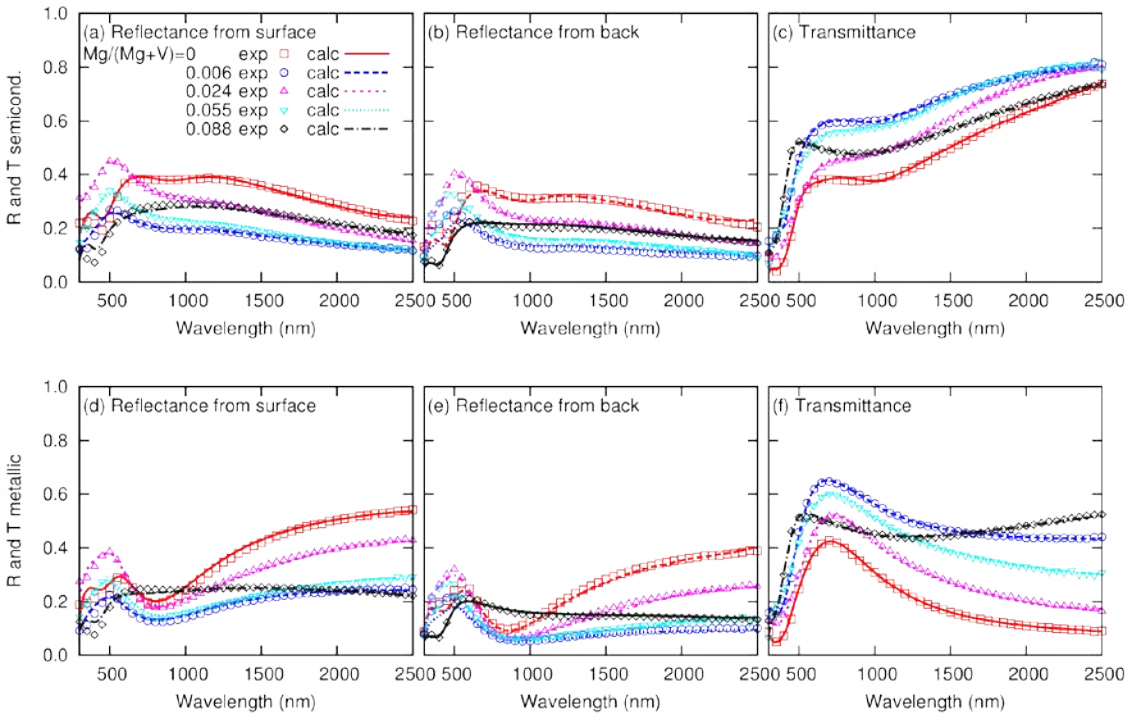
(a) Reflectance from surface
(b) Reflectance from back
(c) Transmittance
Mg/(Mg+V)=0 exp calc
0.006 exp calc
0.024 exp calc
0.055 exp calc
0.088 exp calc
R and T semicond.
(d) Reflectance from surface
(e) Reflectance from back
(f) Transmittance
R and T metallic
Wavelength (nm)

FIG. 3.

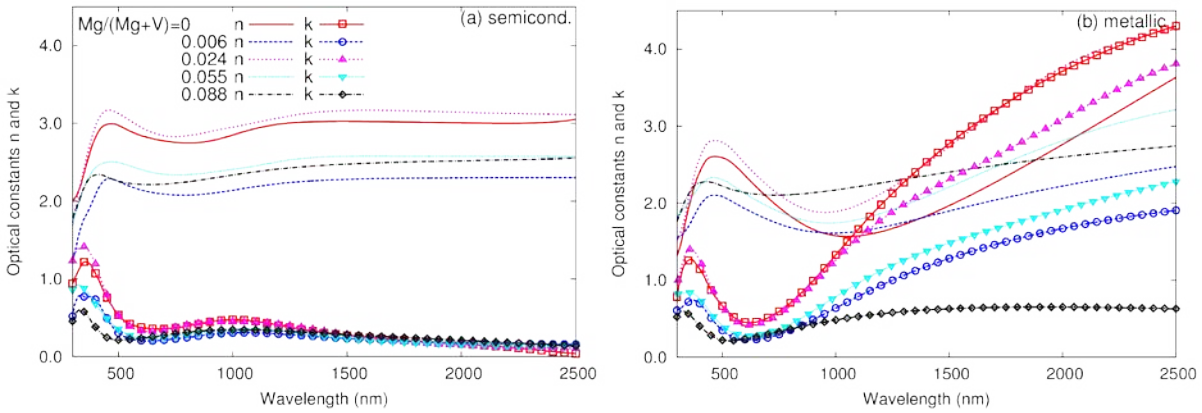
Mg/(Mg+V)=0 n k
0.006 n k
0.024 n k
0.055 n k
0.088 n k
(a) semicond.
(b) metallic
Optical constants n and k
Wavelength (nm)
0.0
1.0
2.0
3.0
4.0
500
1000
1500
2000
2500

FIG. 4.

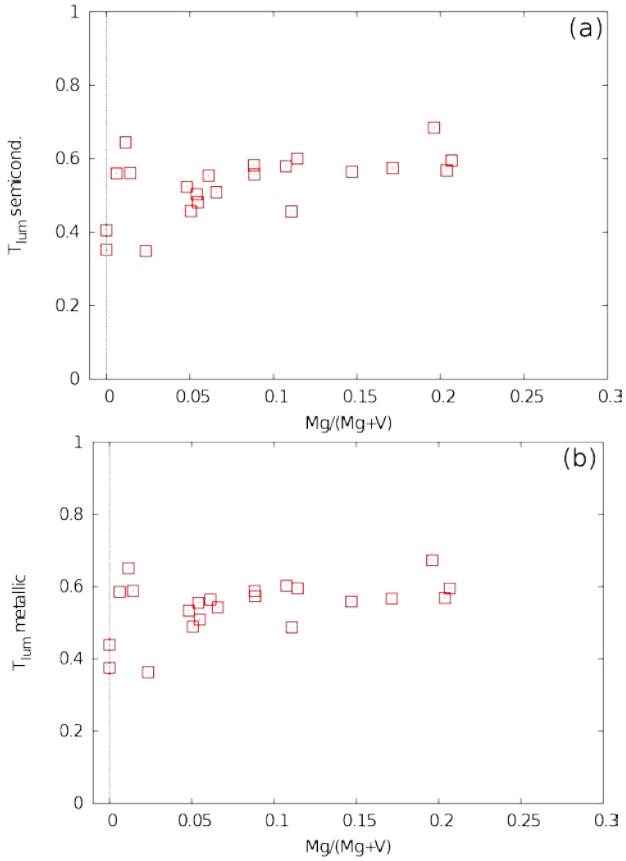
(a)
(b)
T_{lum} semicond.
T_{lum} metallic
Mg/(Mg+V)
0
0.2
0.4
0.6
0.8
1
0.05
0.1
0.15
0.2
0.25
0.3

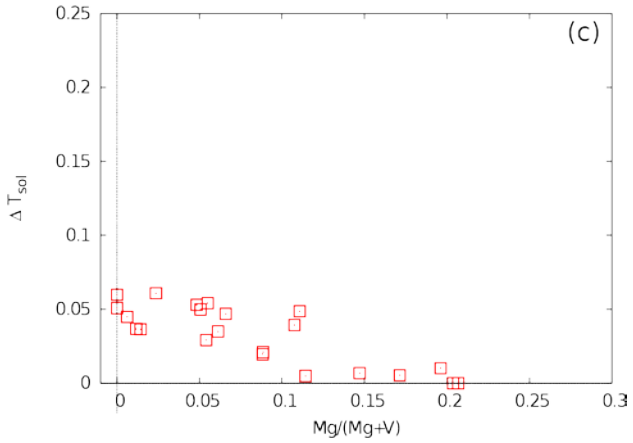
(c)
0.25
0.2
0.15
0.1
0.05
0
Δ T_sol
0
0.05
0.1
0.15
0.2
0.25
0.3
Mg/(Mg+V)

FIG. 5.

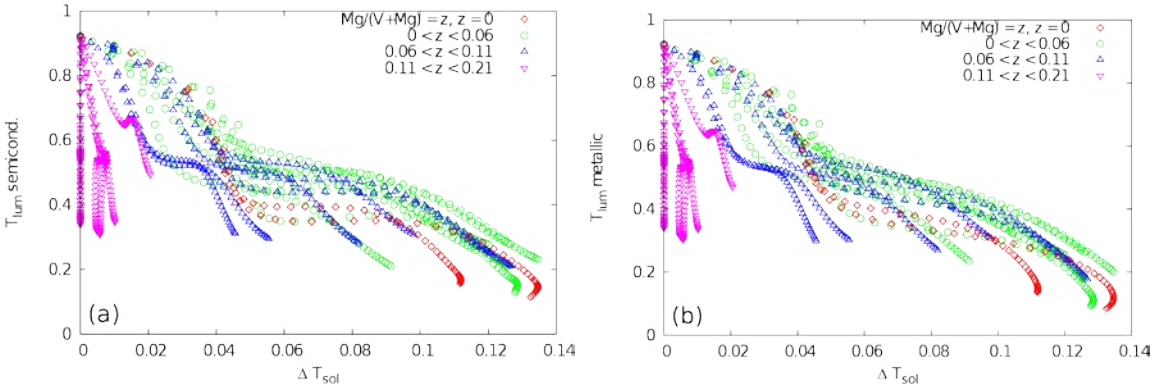
Mg/(V+Mg) = z, z = 0
0 < z < 0.06
0.06 < z < 0.11
0.11 < z < 0.21
(a)
T_lum semicond.
Δ T_sol
(b)
T_lum metallic
Δ T_sol

FIG. 6.

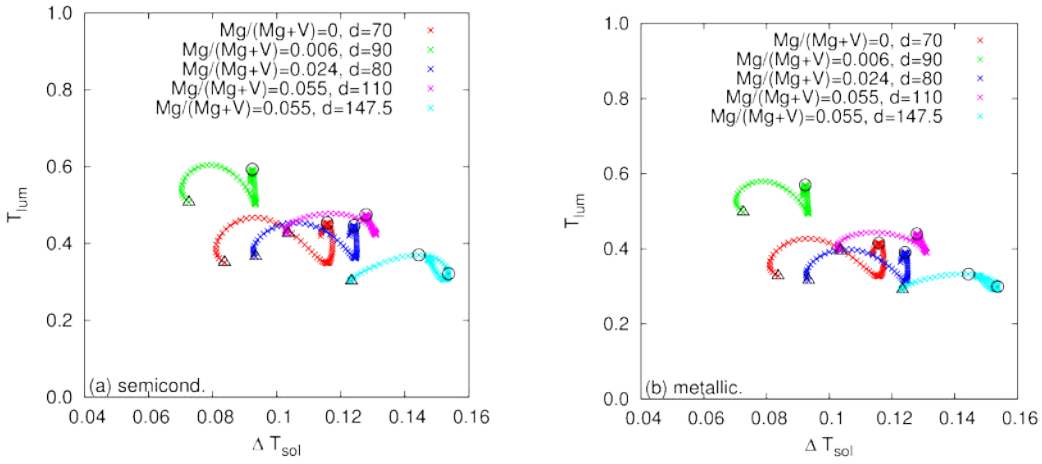
Mg/(Mg+V)=0, d=70
Mg/(Mg+V)=0.006, d=90
Mg/(Mg+V)=0.024, d=80
Mg/(Mg+V)=0.055, d=110
Mg/(Mg+V)=0.055, d=147.5
(a) semicond.
(b) metallic.
T_lum
Δ T_sol

FIG. 7.

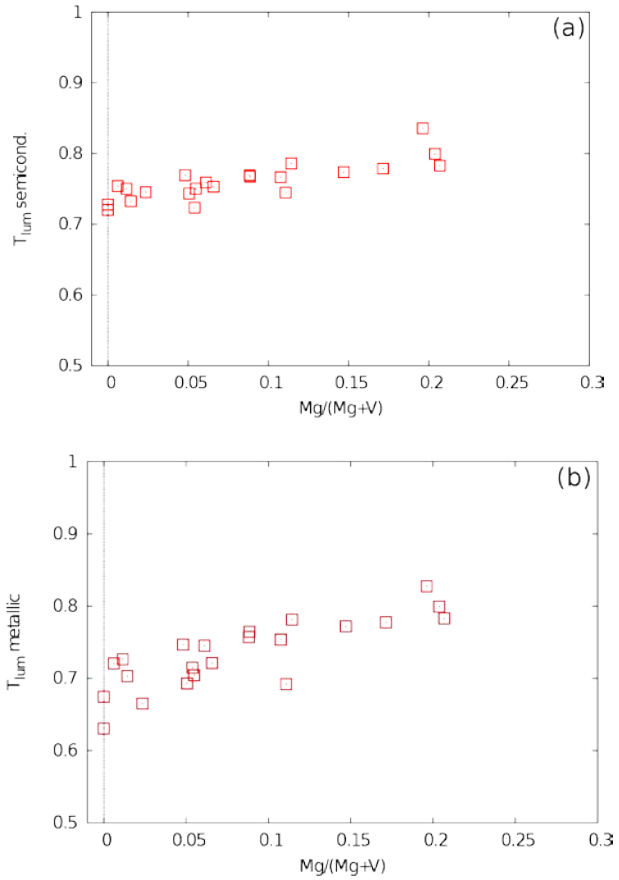
(a)
(b)
T_lum semicond.
T_lum metallic
Mg/(Mg+V)

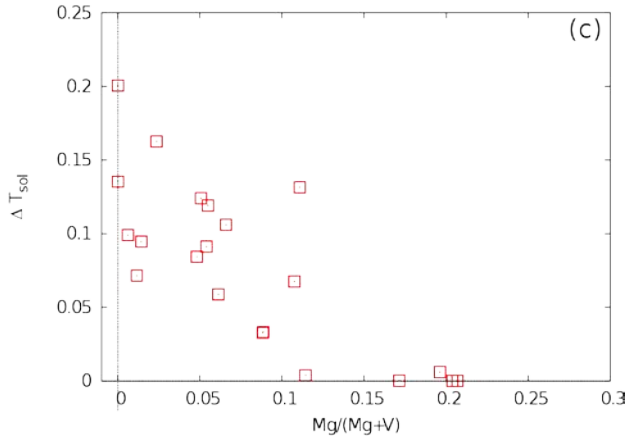

FIG. 8.

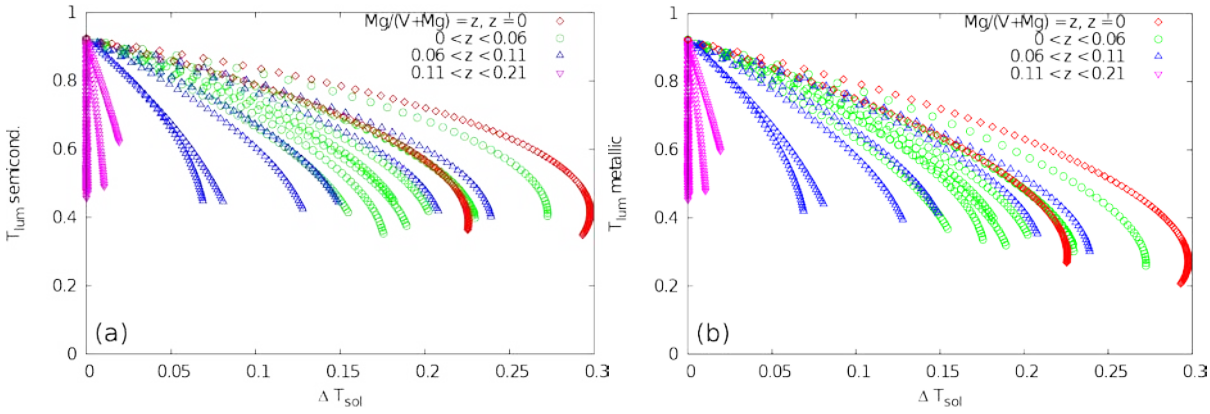

FIG. 9.

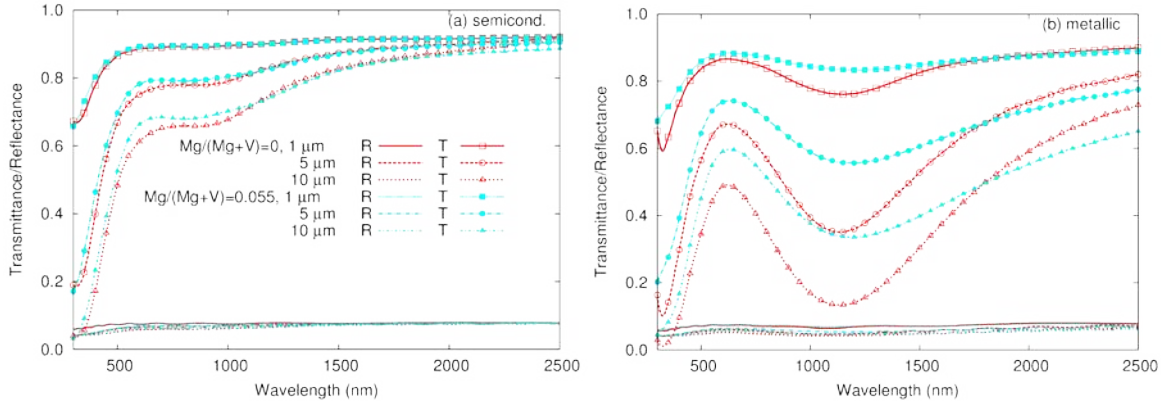

FIG 10.

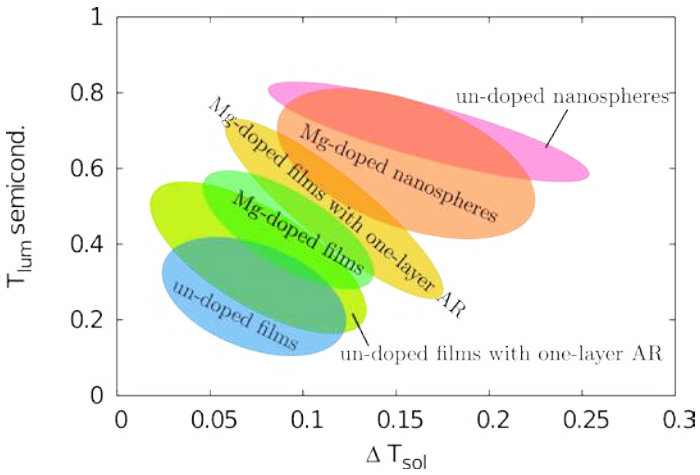
1
0.8
0.6
0.4
0.2
0
0
0.05
0.1
0.15
0.2
0.25
0.3
T_lum semicond.
Δ T_sol
un-doped nanospheres
Mg-doped nanospheres
Mg-doped films with one-layer AR
Mg-doped films
un-doped films
un-doped films with one-layer AR

FIG. 11.